LETTER

doi:10.1038/nature11568

Quasi-periodic events in crystal plasticity and the self-organized avalanche oscillator

Stefanos Papanikolaou[1], Dennis M. Dimiduk[2], Woosong Choi[3], James P. Sethna[3], Michael D. Uchic[2], Christopher F. Woodward[2] & Stefano Zapperi[4,5]

When external stresses in a system—physical, social or virtual—are relieved through impulsive events, it is natural to focus on the attributes of these avalanches[1,2]. However, during the quiescent periods between them[3], stresses may be relieved through competing processes, such as slowly flowing water between earthquakes[4] or thermally activated dislocation flow[5] between plastic bursts in crystals[6–8]. Such smooth responses can in turn have marked effects on the avalanche properties[9]. Here we report an experimental investigation of slowly compressed nickel microcrystals, covering three orders of magnitude in nominal strain rate, in which we observe unconventional quasi-periodic avalanche bursts and higher critical exponents as the strain rate is decreased. Our experiments are faithfully reproduced by analytic and computational dislocation avalanche modelling[10,11] that we have extended to incorporate dislocation relaxation, revealing the emergence of the self-organized avalanche oscillator: a novel critical state exhibiting oscillatory approaches towards a depinning critical point[12]. This theory suggests that whenever avalanches compete with slow relaxation—in settings ranging from crystal microplasticity to earthquakes—dynamical quasi-periodic scale invariance ought to emerge.

Physical systems under slowly increasing stress may respond through abrupt events. Such jumps in observable quantities are abundant, being found in systems ranging from complex social networks to earthquakes. Even though these avalanches appear randomly sized and randomly placed, the statistical properties of avalanches are universal, falling into well understood non-equilibrium universality classes. The main unifying concept is the depinning of an interface under an external field. An implicit assumption underlying this concept is that all other coexisting physical processes are either too fast, and thus average out, or too slow, rendering a static approximation valid. However, the latter assumption is not always true if the slow processes rearrange the pinning landscape at rates comparable to the external field driving rates. For as the fast avalanches are scale-invariant, the whole time series, including the waiting intervals between the fast events, is also scale-invariant. It is within the waiting intervals that a slow restructuring of the pinning field can thrive and alter universal predictions.

Although intermittent plastic flow is well known[13], only recently was it shown as being statistically akin to universal mean-field avalanche behaviour in the quasi-static limit. Investigations of the phenomenon have used a wide variety of techniques, including acoustic emission from deforming ice[6], high-resolution extensometry of tensile strained copper[14], and microcrystal compression tests for face-centred cubic and body-centred cubic crystals[15]. However, most of these single-crystal studies covered only a narrow range of nominal high strain rates. Preliminary evidence that suggests a more complex physical picture was discussed in ref. 16, where a rate dependence of the cumulative strain event size distributions was observed. Interesting rate effects have also been observed in materials with solute atoms, typically polycrystalline, that display the Portevin-Le Chatelier (PLC) effect[17–19]. The PLC avalanche distribution exponents show no evidence of strain-rate dependence (although strain dependence is shown), whereas PLC at lower rates turns into similar-size localized slip excitations and chaotic behaviour[20], distinctly different from the physical behaviour observed in ref. 16. Instead, the PLC avalanche behaviour is more consistent with the phenomenology of theories of avalanches with weakening effects[21]. In the experiments we report here, single nickel microcrystals of comparatively large dimensions, having diameters between 18 and 30 μm, were uniaxially compressed[15]. By controlling the applied external stress to maintain a nominal strain rate and by detecting slip with extremely sensitive extensometry, we track crystal displacements in time. In order to study the rate dependence, we perform our experiments at three different nominal strain rates ($10^{-4}\,s^{-1}$, $10^{-5}\,s^{-1}$, $10^{-6}\,s^{-1}$). For each sample, the time series of the displacement time derivative is filtered using optimal Wiener filtering methods adapted for avalanche time series[22], and avalanche events are appropriately defined without using thresholding.

As deformation proceeds in the microcrystals, the dislocation ensemble evolves at different timescales. The most apparent activity is associated with fast glide processes, which produce stochastic plastic bursts. Concurrently and between these events, other less observable processes (Fig. 1) contribute to collective slower relaxations. Like glide, these too are thermally activated processes accessible at these high levels of stress, but have different activation barriers: for example, the viscoelastic response of the dislocation forests after fast avalanche strain bursts, the localized dislocation climb motion in directions other than the glide plane under high local stresses, and also the cross-slip processes of dislocations shifting between glide planes. They all compete to minimize the far-field stress while changing the local stress landscape and bypassing the fast glide process. They affect dislocation slip, but at a slower rate than avalanche glide[23]. In our experiments, we classify as 'slow relaxation' all the deformation that does not belong to avalanches of the scaling regime. Using this definition, the slow relaxation fraction increases drastically at the two slowest strain rates. Thus, rate dependence of the avalanche size distribution (Fig. 2c) occurs when the nominal strain-rate becomes comparable to the rate of the slow relaxation processes (Fig. 1). Although the exact mechanisms are unknown, one localized reorganization mechanism possible at these large local stresses and low temperatures (0.17 times the melting temperature, ~300 K)[23] could be tied to newly discovered unconventionally large cross-slip rates calculated for similar conditions to our experiments[24]. Regardless of the possible types of relaxation mechanisms, we focus on the experimental fact that relaxation and driving rates become comparable. We model phenomenologically the slow relaxation in an intuitive manner, and then show a posteriori that our results are independent of the particular form of relaxation dynamics (see Supplementary Information).

The slip event sizes S, labelled by their beginning time, display a striking dependence on the driving rate. After we smooth the time

[1]Department of Mechanical Engineering and Materials Science and Department of Physics, Yale University, New Haven, Connecticut 06520-8286, USA. [2]Air Force Research Laboratory, Materials and Manufacturing Directorate, AFRL/RXCM, Wright-Patterson AFB, Ohio 45433, USA. [3]Laboratory of Atomic and Solid State Physics, Department of Physics, Clark Hall, Cornell University, Ithaca, New York 14853-2501, USA. [4]CNR–Consiglio Nazionale delle Ricerche, IENI, Via R. Cozzi 53, 20125 Milano, Italy. [5]ISI Foundation, Via Alassio 11/c, 10126 Torino, Italy.

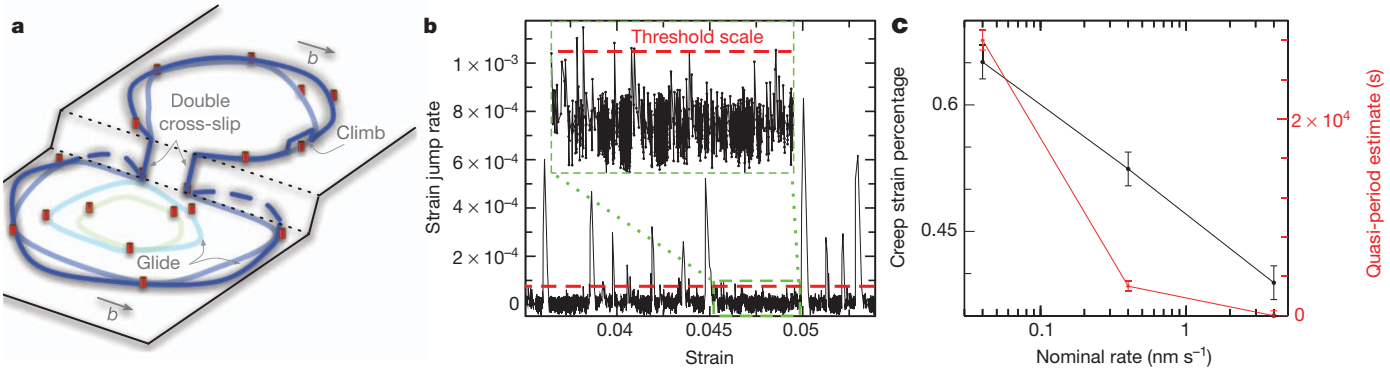

Figure 1 | Dislocation motion and several slow relaxation processes during the waiting intervals between avalanches. **a**, Diagram of typical unit dislocation motions. Lighter to darker indicates time evolution. Under stress, a dislocation loop nucleates and grows until it gets pinned on its slip plane, which is a common and fast glide-slip burst unit process. Then, a screw dislocation segment undergoes double cross-slip to a parallel slip plane, bypassing glide barriers. Finally, the dislocation glides and ultimately, may climb. These unit processes underlie the dislocation ensemble dynamics (not shown). **b**, Strain jump rate time series of a nickel sample at a strain rate of $10^{-6}\,s^{-1}$. The avalanche phenomenon not only involves fast and violent scale-invariant bursts[24], but also long waiting times[3] between glide events. During those times, slow relaxation events happen that are typically hard to experimentally distinguish due to the external noise levels (inset). **c**, Black data points show the estimated strain percentage accumulated in slow relaxation events (generally called 'creep'), with the threshold set by the event size distribution (Fig. 2): this percentage (relaxation strain/total final strain) strongly increases as the rate decreases. Experimental noise contributes to the relaxation strain measured. Red data points show that a non-trivial quasi-period (see Fig. 2) of avalanche behaviour emerges and increases dramatically as the nominal rate decreases. Error bars indicate the size of systematic variability due to thresholding.

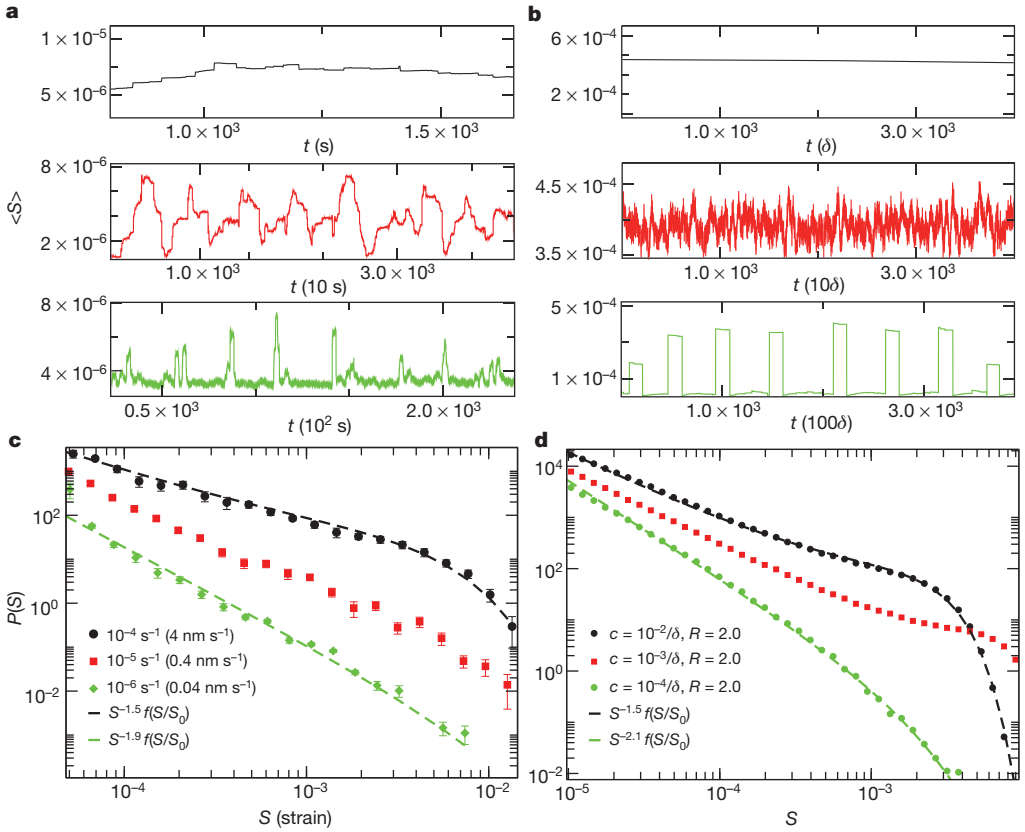

Figure 2 | Comparison between microplasticity experiments and theoretical modelling. **a**, Average avalanche size in 400-s windows versus time for different strain rates (decreasing top to bottom: 10^{-4}, 10^{-5}, $10^{-6}\,s^{-1}$, corresponding to respective velocities of the microcrystal top surfaces of 4, 0.4, 0.04 nm s^{-1}). Time axes are rescaled by the nominal strain rate, aligning the 'strain scales'. Quasi-periodic avalanche behaviour emerges as the nominal strain rate decreases. The period is similar in 'strain scale'—a key prediction of our theory. **b**, Stick-slip oscillations observed experimentally in **a** show typical characteristics of the model of equation (1) (using 400δ-long averaging windows). The relaxation rate is fixed ($R = 2$) and the strain-rate is varied (by modifying c: top to bottom; $10^{-2}/\delta$, $10^{-3}/\delta$, $10^{-4}/\delta$), following the experiments. The unit of strain is 2×10^{-6} and the fast timescale $\delta = 0.5$ s. We show the actual avalanche events without the distortion that appears due to the strain coming from slow relaxation; this difference gives the overall scale mismatch of **a** and **b**. **c**, The probability distribution $P(S)$ is shown. There is a marked increase in the critical exponent for the size of the displacement jumps as the strain rate decreases. The highest (10^{-4}) and lowest (10^{-6}) strain rates are fitted to power laws $S^{-1.5}f(S/S_0)$ and $S^{-1.9}f(S/S_0)$, respectively. The key shows strain rate and corresponding velocity for data points. **d**, In the model of equation (1), the variation of the rate c shows similar behaviour to that observed in **c**, with exponent drift from ~1.5 (ref. 8) to ~2.1, with fitting error ~0.2, consistent with the discussion in the text and with fitting cut-off functional forms $f(S/S_0)$ that are discussed in Methods.

series over a fixed window of 400 s and then rescale the time axis to display comparable strain evolution, very clear (Fig. 2a) oscillatory-like behaviour emerges at the $10^{-6}\,s^{-1}$ rate. The emergent period displays a strong dependence on the strain rate, while its magnitude reaches ~8 h (for $10^{-6}\,s^{-1}$), consistently much larger than the length we chose for the fixed window averaging (Fig. 1c). The novel behaviour is also reflected within statistical distributions of S: these show power-law behaviour ($P(S) \propto S^{-\tau}$) for all studied strain rates ($10^{-4}\,s^{-1}$, $10^{-5}\,s^{-1}$, $10^{-6}\,s^{-1}$), while the value of the power law exponent τ drifts from ~1.5 (consistent with refs 7 and 25) to a higher, unexpected value of ~2.0 for the slowest strain rate (Fig. 2c). Analogous behaviour is observed for the avalanche durations T and their correlation with the sizes.

Our explanation of the experimental data builds on the model framework of dislocations moving through a disordered landscape of forest dislocations, on a single slip plane under shear stress. This is a successful picture for avalanches during stage I plasticity[10,11,25] that strongly relies on well-understood models of 2+1-dimensional interface depinning[12]. We construct a minimal generalization via an added relaxation term, (I):

$$\frac{d\phi(r)}{dt} = \overbrace{D\left(\frac{\sigma(r)}{\mu}\right)^{n}\Theta(\sigma(r))}^{(I)} + \overbrace{\frac{1}{\mu\varepsilon}(\sigma(r)-\sigma_f(r))\Theta(\sigma(r)-\sigma_f(r))}^{(II)} \quad (1)$$

Here r denotes the location on the slip plane, t is time, Θ is the Heaviside step function, μ is the shear modulus of the system, $\varepsilon \ll 1$ is a dimensionless constant that controls the timescale separation of the two processes (I) and (II), n is the stress exponent dependent on the slow relaxation mechanism, σ is the local applied stress and σ_f denotes random stress barriers to glide slip. The basic slip variable of the system ϕ is the y–x component (Burgers vector along x) of the plastic distortion tensor when only infinite dislocations along z on x–z slip planes are considered[10]. Part (I) of equation (1) denotes the coarse-grained relaxation of edge dislocations, with rate D at fixed temperature. Only positive slip motion is considered to simplify our simulations, and we have shown that our conclusions are qualitatively independent of such assumptions (see Supplementary Information). With D we define an effective rate of thermally activated processes that lead to slow relaxation. We set the exponent $n = 1$ but our conclusions do not qualitatively depend upon it. The applied stress is the x–y component of the stress tensor:

$$\sigma(r) = \sigma_{ext} + \sigma_{int}(r) + \sigma_{hard}(r) = Mct + \int d^2r' K(r-r')\phi(r') - k\phi(r) \quad (2)$$

where σ_{ext} is the external stress with c the stress increase rate, σ_{int} is the dislocation local stress, σ_{hard} is the local stress due to dislocation hardening with k a phenomenological hardening parameter, and r' is defined on the slip plane.

We consider a stress-controlled test in a stationary plastic regime ($\sigma_{ext} \equiv Mct$)[26], where M is a machine stiffness, and c has strain-rate units. The relative timescales of the relaxation and stress rate are controlled by the dimensionless parameter $R \equiv D/c$. Term (II) of equation (1) describes the fast glide process which drives the avalanche dynamics. Hardening is phenomenologically represented via a coefficient k that controls the distance from the depinning critical point. For clarity, we separate the relevant timescales by considering $\varepsilon \ll 1$, leading to infinitely fast avalanches compared to the slow relaxations. Finally, σ_{int} contains the appropriate interaction kernel K for single slip straight edge dislocations[10] and σ_f denotes the uncorrelated local pinning potential due to dislocation forests. We find that our main qualitative conclusions are independent of the kernel, and thus are equally applicable to other models of avalanches in plasticity. If we were considering the model of ref. 11 where mixed dislocations are included, we would modify our definitions by using a single x–y slip plane, assume ϕ to be the x–y tensor component, and only apply the z–x component of the stress.

The model of equations (1) and (2) is solved by explicit integration on a two-dimensional grid: for no relaxation ($D = 0$), the avalanches display statistics consistent with the predictions of the mean-field theory of interface depinning[2,8]. As D increases, both the critical exponent τ for strain jump sizes S ($P(S) \propto S^{-\tau}$) and the critical exponent α for event durations T ($P(T) \propto T^{-\alpha}$) increase substantially. In the context of mean-field theory, somewhat similar behaviour takes place when the driving rate c is increased[22], leading to avalanche overlap and exponents decreasing below the mean-field values; we study the case where $c \to 0$, keeping R fixed (and >1) where the exponents increase above their mean-field values.

The increase of the exponents is accompanied by a quasi-periodic behaviour, with intermittent but regularly spaced large slip events (Fig. 2b), keeping in mind that the term quasi-periodic is unrelated to the formal definition of quasiperiodic functions. If one considers the average avalanche size in a window, similar to the experimental study but without strain from relaxation included, it is clear that the $D = 0$ flat-in-time profile is replaced by strongly oscillating profiles in the presence of slow relaxation ($D > 0$). The average avalanche size ($D = 0$) is inversely related to the hardening coefficient k, $k \propto <S>^{-1}$. Thus, there is a distribution of hardening coefficients being effectively sampled, reflecting local heterogeneity. We assume that such a distribution $g(k')$ biases the integration, over all possible hardenings k', of the size probability distribution of the $D = 0$ model, leading to the observed dynamically integrated size distribution. That is, a curve in Fig. 2d may be obtained as:

$$P_{int}(S) = \int_0^\infty g(k')P(S,k')dk' \quad (3)$$

For the case of interest we have $P_{int}(S) = S^{-2}P(S/S_0)$, where S_0 is the cutoff of the size distribution, yielding a higher effective size-exponent $\tilde{\tau} \equiv 2$ for slow strain rates. It is worth noting that in this picture, the largest events have a non-trivial scaling behaviour (see Supplementary Information).

The profound effects of slow rate processes within our dislocation model and the comparison with experiments forces us to ask if our findings are general. To make analytical progress towards an answer, we consider the slip susceptibility ρ, the multiplier giving the net number of local slips triggered by a single slip. Here, $\langle\rho\rangle$ is proportional to the hardening coefficient, $\langle\rho\rangle \propto 1 - k$. In traditional mean-field interface depinning models[1], this is the 'distance' of the system from the critical depinning point and is saturated to a fixed point value after short-time transients. When $\rho \ll 1$, the system is far from critical, whereas the system is near critical when $\rho \approx 1$. Numerical solutions to equation (1) verify that the additional relaxation process affects ρ in an unusual way. When an avalanche with size S_t takes place, ρ instantaneously decreases proportionally to S_t, whereas it increases linearly between avalanches. We suggest that the basic physical mechanism behind the behaviour of equation (1) (with $c \to 0$ but R fixed) is given by the behaviour of the slip susceptibility ρ, whose basic characteristics can be described by a Markov process:

$$\rho_{t+1} - \rho_t \equiv \Delta\rho_t = c_d\left(1 - \frac{S_t}{\bar{S}}\right) \quad (4)$$

where S_t is mean-field $P(S_t) = NS_t^{-3/2}\exp(-S_t/S_0)$; here N is a normalization factor, $S_0 = a/(1-\rho_t)^2$ (ref. 1) and the step c_d can be thought as being proportional to R. The traditional avalanche mean-field behaviour is described by the $c_d \to 0$ fixed point (analogous to higher experimental strain rates). The size of the avalanche at time t, S_t, is a stochastic variable which mimics the avalanche dynamics of

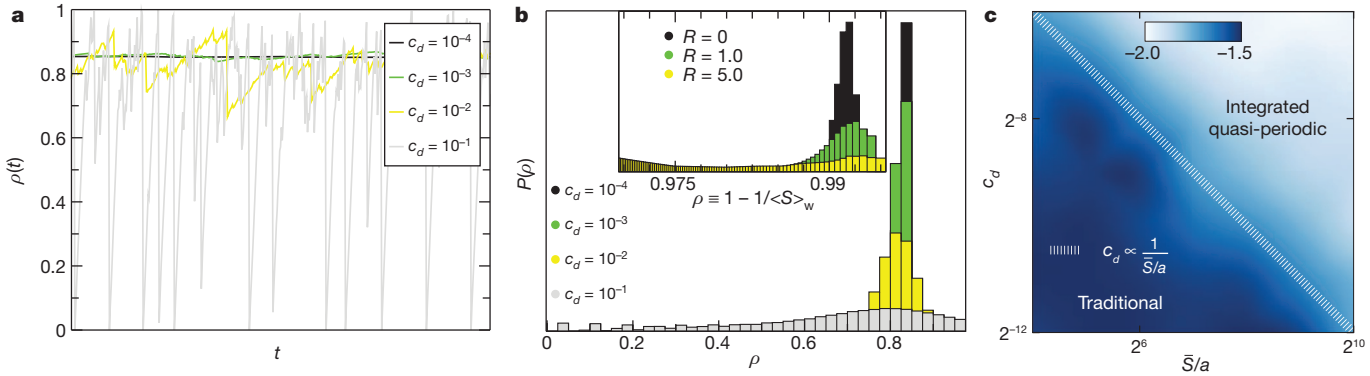

Figure 3 | The avalanche oscillator mechanism and stochastic modelling of the slip susceptibility. **a**, As the rate c_d increases (key), for $\bar{S} = 0.1$, large noise causes $\rho(t)$ of equation (4) to oscillate between $\rho \approx 1$ and small ρ, causing larger exponents. **b**, The probability distribution of ρ. As c_d increases (stronger relaxation, slower strain rate), any ρ becomes equiprobable. In the inset, we use $\langle S \rangle_{50}$ calculated for equation (1), averaged with a running window of size 50δ. The simulations of equation (1) have the same parameters as in Fig. 2. The histograms, shown in the appropriate scale ($1 - 1/\langle S \rangle \equiv \rho$ for the kernel used) shows qualitatively similar flattening behaviour as equation (4). **c**, The novel regime ('integrated quasi-periodic') with large ρ fluctuations is separated from the traditional regime $\rho \approx \rho_0$. The line $c_d \propto 1/\bar{S}$ shown, as described in the text. $\tilde{\tau}$ was calculated using equation (3) at equidistant points with a final Gaussian interpolation for the colour background.

equation (1). When $c_d \ll 1$, ρ increases in small steps towards the fixed point (Fig. 3a) given by $\rho_0 = 1 - (\sqrt{\pi a}/2\bar{S})$ with average size $\bar{S}$ (a being the minimum accessible size).

However, there is a finite probability of a large avalanche which takes the system far from the fixed point, with $\Delta\rho_t$ large and negative. If $\delta S = S_t - \bar{S}$, then $\Delta\rho_t = -c_d \delta S/\bar{S} \approx -1$ indicates the emergence of a novel quasi-periodic behaviour (Fig. 1b) showing large negative jumps in ρ with rare avalanches whose sizes S_t are much larger than $\bar{S}$. ρ performs a Sisyphean task, constantly ascending towards the original critical point ρ_0 before the sharp descent after a large rare avalanche. In this way, the distribution of ρ effectively flattens (Fig. 3b) as c_d increases (low experimental strain rates), leading to larger integrated exponents (equation (3)). Consistently, the analogous distribution for equation (1) flattens as R increases (Fig. 3b, inset). The rare δS events scale with $S_0 \propto 4\bar{S}^2/(\pi a)$ and qualitatively, there is a transition when $c_d \approx a\pi/(4\bar{S}) \approx 1/(\bar{S}/a)$ (Fig. 3c). We call a system undergoing this qualitative behaviour an 'avalanche oscillator', based on its strong resemblance to the case of relaxation limit cycle oscillations near a singular Hopf bifurcation with stochastic perturbations[27].

Single microcrystals display a rich collection of novel mechanical behaviours: together with size effects[15] and the emergence of avalanche slip events[6,7], the importance of often-neglected slow processes on intermittency has now come to light. The presented experiments at the microscale now force us to reconsider our understanding of the macroscopic world, such as disordered solids and earthquake faults[28–30]. Our general theory proposes that whenever avalanches compete with other slow coexisting processes to minimize the local internal stress, the dynamics will give rise to the self-organized avalanche oscillator.

METHODS SUMMARY

The experimental measurements were performed using the methodology described earlier[15,16]. The data are taken at time resolutions of 5, 50 and 500 Hz for different samples. The nominal strain rates (in s^{-1}) were 10^{-4}, 10^{-5} and 10^{-6}, with corresponding average platen velocities of 4, 0.4 and 0.04 nm s^{-1}, given the dimensions of the microcrystals. The experimental time series were filtered using Wiener filtering methods optimized for studying avalanches[22]. In the simulations of equation (1), Euler time stepping is used to evolve the differential equation on an $L \times L$ grid. During an avalanche, the stress is not increased and the relaxation term (I) does not participate in the evolution. During the avalanche process, we evolve the system by using cellular automata rules: when the total local stress crosses its σ_f threshold, the associated local slip ϕ increases randomly with a normal distribution of mean 1 and variance 1. The assumption of strict positivity in the local slip is used for simulation efficiency purposes, without affecting our conclusions. In the stress of equation (1), we have also added a term for regularizing purposes that slightly smooths the slip profiles. It takes the form $\alpha\nabla^2\varphi$ with very small $\alpha = 0.05$. In our simulations, we used a flat distribution ranged in (0,1] for the quenched disorder $\sigma_f(r)$, following a typical protocol. The kernel $K(r)$ has a continuum Fourier representation $\tilde{K}(k) = -Ck_x^2k_y^2/(k_x^2 + k_y^2)^2$, where we set $C = 1$ for clarity in our analysis. In the simulations of equation (4), the stochastic equation was solved using random variables that follow the required power-law distribution with exponential cut-off, generated with standard rejection methods. During the numerical solution of equation (4), ρ can jump above 1, a regime we do not consider (see Supplementary Information).

Full Methods and any associated references are available in the online version of the paper.

Received 24 February; accepted 5 September 2012.

1. Fisher, D. S. Collective transport in random media: from superconductors to earthquakes. *Phys. Rep.* **301,** 113–150 (1998).
2. Sethna, J., Dahmen, K. & Myers, C. Crackling noise. *Nature* **410,** 242–250 (2001).
3. Le Doussal, P. & Wiese, K. J. Driven particle in a random landscape: disorder correlator, avalanche distribution, and extreme value statistics of records. *Phys. Rev. E* **79,** 051105 (2009).
4. Ben-Zion, Y. Collective behavior of earthquakes and faults: continuum-discrete transitions, progressive evolutionary changes and different dynamic regimes. *Rev. Geophys.* **46,** RG4006 (2008).
5. Cottrell, A. H. *Dislocations and Plastic Flow in Metals* (Clarendon, 1953).
6. Miguel, M. C., Vespignani, A., Zapperi, S., Weiss, J. & Grasso, J.-R. Intermittent dislocation flow in viscoplastic deformation. *Nature* **410,** 667–671 (2001).
7. Dimiduk, D. M., Woodward, C., LeSar, R. & Uchic, M. D. Scale-free intermittent flow in crystal plasticity. *Science* **312,** 1188–1190 (2006).
8. Zaiser, M. Scale invariance in plastic flow of crystalline solids. *Adv. Phys.* **55,** 185–245 (2006).
9. Jagla, E. A. Realistic spatial and temporal earthquake distributions in a modified Olami-Feder-Christensen model. *Phys. Rev. E* **81,** 046117 (2010).
10. Zaiser, M. & Moretti, P. Fluctuation phenomena in crystal plasticity—a continuum model. *J. Stat. Mech.* **2005,** P08004 (2005).
11. Koslowski, M., LeSar, R. & Thomson, R. Avalanches and scaling in plastic deformation. *Phys. Rev. Lett.* **93,** 125502 (2004).
12. Kardar, M. Nonequilibrium dynamics of interfaces and lines. *Phys. Rep.* **301,** 85–112 (1998).
13. Becker, R. & Orowan, E. Uber sprunghafte Dehnung von Zinkkristallen. *Z. Phys.* **79,** 566–572 (1932).
14. Weiss, J. *et al.* Evidence for universal intermittent crystal plasticity from acoustic emission and high-resolution extensometry experiments. *Phys. Rev. B* **76,** 224110 (2007).
15. Uchic, M. D., Dimiduk, D. M. & Shade, P. A. Plasticity of micrometer-scale single crystals in compression. *Annu. Rev. Mater. Res.* **39,** 361–386 (2009).
16. Dimiduk, D. M., Uchic, M. D., Rao, S. I., Woodward, C. & Parthasarathy, T. A. Overview of experiments on microcrystal plasticity in FCC-derivative materials: selected challenges for modelling and simulation of plasticity. *Model. Simul. Mater. Sci. Eng.* **15,** 135–146 (2007).
17. Lebyodkin, M., Dunin-Barkowskii, L., Bréchet, Y., Estrin, Y. & Kubin, L. P. Spatio-temporal dynamics of the Portevin–Le Chatelier effect: experiment and modelling. *Acta Mater.* **48,** 2529–2541 (2000).
18. Kubin, L. P. *et al.* in *Dislocations in Solids* (eds Nabarro, F. R. N. & Duesberry, M. S.) Ch. 57, 103–188 (North Holland, 2002).
19. Bharathi, M. S., Lebyodkin, M., Ananthakrishna, G., Fressengeas, C. & Kubin, L. P. The hidden order behind jerky flow. *Acta Mater.* **50,** 2813–2824 (2002).

20. Lebyodkin, M. A. *et al.* On the similarity of plastic flow processes during smooth and jerky flow: statistical analysis. *Acta Mater.* **60,** 3729–3740 (2012).
21. Fisher, D. S., Dahmen, K., Ramanathan, S. & Ben-Zion, Y. Statistics of earthquakes in simple models of heterogeneous faults. *Phys. Rev. Lett.* **78,** 4885–4888 (1997).
22. Papanikolaou, S. *et al.* Universality beyond power laws and the average avalanche shape. *Nature Phys.* **7,** 316–320 (2011).
23. Kassner, M. & Perez-Prado, M.-T. *Fundamentals of Creep in Metals and Alloys* (Elsevier, 2004).
24. Rao, S. I. *et al.* Activated states for cross-slip at screw dislocation intersections in face-centered cubic nickel and copper via atomistic simulation. *Acta Mater.* **58,** 5547–5557 (2010).
25. Csikor, F. F., Motz, C., Weygand, D., Zaiser, M. & Zapperi, S. Dislocation avalanches, strain bursts, and the problem of plastic forming at the micrometer scale. *Science* **318,** 251–254 (2007).
26. Zaiser, M. & Nikitas, N. Slip avalanches in crystal plasticity: scaling of the avalanche cut-off. *J. Stat. Mech.* **2007,** P04013 (2007).
27. Muratov, C. & Vanden-Eijnden, E. Noise-induced mixed-mode oscillations in a relaxation oscillator near the onset of a limit cycle. *Chaos* **18,** 015111 (2008).
28. Rogers, G. & Dragert, H. Episodic tremor and slip on the Cascadia subduction zone: the chatter of silent slip. *Science* **300,** 1942–1943 (2003).
29. Salerno, K. M., Maloney, C. E. & Robbins, M. O. Avalanches in strained amorphous solids: does inertia destroy critical behavior? Preprint at http://arxiv.org/abs/1204.5965 (2012).
30. Dahmen, K. A., Ben-Zion, Y. & Uhl, J. T. A simple analytic theory for the statistics of avalanches in sheared granular materials. *Nature Phys.* **7,** 554–557 (2011).

Supplementary Information is available in the online version of the paper.

Acknowledgements We thank J. Guckenheimer, C. L. Henley, E. A. Jagla, E. Nadgorny, C. O'Hern, R. Thorne, D. Trinkle, E. van der Giessen and V. Vitelli for discussions. We acknowledge support from DTRA 1-10-1-0021 (S.P.), DOE-BES DE-FG02-07ER-46393 (S.P., W.C. and J.P.S.), the Air Force Office of Scientific Research (D. Stargel) and the Materials and Manufacturing Directorate (D.M.D., C.F.W. and M.D.U.) and the ComplexityNet pilot project LOCAT (S.Z.).

Author Contributions D.M.D., M.D.U. and C.F.W. designed and performed the experiments. S.P., D.M.D. and C.F.W. performed the experimental data analysis. S.P., W.C., J.P.S. and S.Z. developed the theoretical modelling, performed the numerical simulations and carried out the data analysis. S.P. wrote the first draft of the manuscript and then all authors contributed equally to improve the manuscript.

Author Information Reprints and permissions information is available at www.nature.com/reprints. The authors declare no competing financial interests. Readers are welcome to comment on the online version of the paper. Correspondence and requests for materials should be addressed to S.P. (stefanos.papanikolaou@yale.edu).

METHODS

Experimental. The data are taken at time resolutions 5, 50 and 500 Hz for different samples, depending on the case. The nominal strain rates were 10^{-4}, 10^{-5}, $10^{-6}\,s^{-1}$ with corresponding average platen velocities of 4, 0.4 and 0.04 nm s^{-1}, given the dimensions of the pillars. Optimal Wiener filtering corresponds to a low-pass filter that has significant effects only at short timescales, which are plagued by apparatus problems. In a similar fashion to ref. 24, we performed adequate tests in order to confirm that the power-laws and the long-time quasi-periodic behaviour were not related to the filtering procedure.

Theoretical. In the simulations of equation (1), during diffusion, Euler time stepping is used to evolve the differential equation on a $L \times L$ grid. During an avalanche, given that $\varepsilon \to 0$, the stress is not increased and the relaxation term (I) does not participate in the evolution. This approximation was performed for clarity purposes, with qualitatively similar results with the case $\varepsilon = 1$. In that case, the effect of diffusion is more visible and avalanches dissipate (for large D) a much smaller stress percentage, since the relaxation term dominates the behaviour. During the avalanche process, we evolve the system by using cellular automata rules: when the total local stress crosses its σ_f threshold, the associated local slip ϕ increases randomly with a normal distribution with mean 1 and variance 1. The assumption of strict positivity in the local slip is used for simulation efficiency purposes, without affecting our conclusions, as we demonstrate in Supplementary Information[31]. In the stress of equation (1), we have also added a term for regularizing purposes that slightly smoothens the slip profiles. It takes the form $\alpha\nabla^2\phi$ with very small $\alpha = 0.05$. We have checked for several system sizes (up to 64^2) that this term does not affect our reported results in any visible manner. Also, we note that this term is physically motivated, in as much as it is connected to the coarse-grained form of the stress generated by dislocation pile-ups[8]. In our simulations we used a flat distribution ranged in (0,1] for the quenched disorder $\sigma_f(r)$, following a typical protocol. The kernel $K(r)$ has a continuum Fourier representation $\tilde{K}(k) = -Ck_x^2k_y^2/(k_x^2 + k_y^2)^2$ (ref. 10), where we set $C = 1$ for clarity purposes in our analysis. A modification of C modifies the strength of disorder required in the model in order to observe avalanche behaviour, with no other changes. In all simulations using equation (1) (unless explicitly mentioned otherwise) the hardening coefficient k is selected from the formula $k = 2L^{0.85}/S_0$ where we chose $S_0 = 1{,}000$ with S_0 being approximately equal to the cut-off size of the distribution that is derived for $D = 0$. The reason for this choice has to do with the fact that the nature of the kernel is such that a fixed local hardening coefficient k does not set the cut-off for the size distribution. Rather, it allows for a weak increase with the system size. However, for our purpose (studies of $D > 0$) it was crucial to have well controlled critical distributions for $D = 0$, independent of the system size, to identify the concrete effects of the relaxation on the distributions. In all plots we refer to the value of $R = D/c$. We note that all our conclusions remain qualitatively unaltered if a strain-rate-controlled test is considered, while the only requirement we identified for the emergence of the avalanche oscillator is the existence of a large range of time intervals between distinct events, as self-similarity requires[32]. The independence of the avalanche oscillator behaviour from the external forcing type is in contrast to typical microscopic friction stick-slip[33,34] or coarse-grained weakening[21,35] modelling that lead to stick-slip avalanche periodicity and typical infinite off-critical events[36]. In the simulations of equation (4), the stochastic equation was solved using random variables that follow the required power-law distribution with exponential cut-off, generated with the standard rejection method[37]. While solving equation (4) numerically, ρ can jump above 1, a regime that we do not consider. There are several options to deal with the boundary condition at $\rho = 1$ which are numerically very similar for large $\bar{S}$ and small c_d. After a jump which takes $\rho > 1$: (1) ρ is reset to a random value between 0 and 1; (2) ρ is reset to a specific value (for example, 0 or ρ_0); (3) ρ is returned to its previous value and the step is rejected (this method was used for the generation of Fig. 3 centre). We shall reiterate that these crossings ($\rho > 1$) are regularization/finite-size effects and do not define the system's behaviour at long times and in the limit of $\bar{S}/a \to \infty$, as we verified in both simulations of equation (1) (showing that the distribution 'bump' consistently vanishes with the system size) and equation (4) (showing that different treatments of the $\rho = 1$ boundary lead to the same conclusion and phase boundary $c_d \propto 1/\bar{S}$). Finally, in Fig. 2, the fitting functional forms used were $c_0 S^{-\tau} e^{-c_1(S/S_0)^{c_3} + c_2\sqrt{S/S_0}}$ where c_0, c_1, c_2, c_3 and τ are fitting parameters. As it appears from our theoretical study, the cut-off functions $f(S/S_0)$ are rate dependent. For example, in Fig. 2c, we find $c_3 = 3/2$ at 10^{-4} rate, while it is $c_3 = 1$ at 10^{-6}. In Fig. 2d, $c_3 = 2$ at the low rate, while it is $c_3 = 1$ at the high one.

31. Middleton, A. A. Asymptotic uniqueness of the sliding state for charge-density waves. *Phys. Rev. Lett.* **68,** 670–673 (1992).
32. Corral, A. Point-occurrence self-similarity in crackling-noise systems and in other complex systems. *J. Stat. Mech.* **2009,** P01022 (2009).
33. Burridge, R. & Knopoff, L. Model and theoretical seismicity. *Bull. Seismol. Soc. Am.* **57,** 341–371 (1967).
34. Carlson, J. M., Langer, J. S. & Shaw, B. E. Dynamics of earthquake faults. *Rev. Mod. Phys.* **66,** 657–671 (1994).
35. Ben-Zion, Y., Eneva, M. & Liu, Y. Large earthquake cycles and intermittent criticality on heterogeneous faults due to evolving stress and seismicity. *J. Geophys. Res.* **108,** 2307–2328 (2003).
36. Perković, O., Dahmen, K. A. & Sethna, J. P. Disorder-induced critical phenomena in hysteresis: numerical scaling in three and higher dimensions. *Phys. Rev. B* **59,** 6106–6119 (1999).
37. Press, W. H., Flannery, B. P., Teukolsky, S. A. & Vetterling, W. T. *Numerical Recipes* (Cambridge Univ. Press, 1986).